# VR-based Interactive CFD Data Comparison of Flow Fields in a Human Nasal Cavity

Andreas Gerndt*, Torsten Kuhlen, Thomas van Reimersdahl, Matthias Haack, Christian Bischof
Center for Computing and Communication, Aachen University (RWTH),
Seffenter Weg 23, 52074 Aachen, Germany

## ABSTRACT

The Virtual Reality Center Aachen is developing a Virtual Reality based operation planning system in cooperation with aerodynamics scientists and physicians of several clinical centers. This system is meant to help the preparation of nose surgeries aimed at the elimination of respiratory diseases. A core part is the interactive comparison of experimental data and simulation data in the area of fluid dynamics. In a first step, data comparison is to depict the differences between healthy noses and diseased noses. Later on, data comparison should supply evidence for successful virtual surgeries, which finally results in guidance on the real operation.

During virtual surgery sessions, scientists can interactively explore, analyze, annotate, and compare various medical and aerodynamics data sets. Image-based methods are used to extract several features in one image and between compared data sets. The determination of linked features between different data sets is a particular challenge because of their different time frames, scales, and distortions. An optimized human computer interface enables the user to interact intuitively within a virtual environment in order to select and deal with these data sets. Additionally to this interactive exploration, the system also allows automatic searches for cut plane and key frame candidates corresponding to given feature patterns.

The comparison system makes use of an already implemented parallelized Computational Fluid Dynamics (CFD) post-processing, which also extracts enhanced flow features that allow automatic detection of relevant flow regions. Beside vortex detection, the computation of critical points including flow field segmentation is a current research activity. These flow features are favored characteristics for the comparison and help considerably to classify different nose geometries and operation recommendations.

**Keywords:** Virtual Reality, Computational Fluid Dynamics, Surgery Planning System, Experiment – Simulation Comparison, Flow Feature Extraction

## 1. INTRODUCTION

The human nose covers a variety of physiological functions. Mainly, it is warming, moistening and filtering the inhaled air. Additionally, located in the upper region of the nose cavity, the olfactory system is responsible for the sense of smell. All these functions considerably depend on flow conditions within the nose cavity. Due to injuries, deformity or diseases, respiration can be restricted. Often, only a nose surgery is capable to remove these complaints.

Nose surgeries are not rare operations; however, many have to be repeated because patients still complain of difficulties in breathing. The reason is that changing the geometry of the nose cavity can modify the flow field substantially; but without knowledge about the aerodynamics within a human nose wrong modifications might be applied. The goal is that only minor operations (if possible) are applied in order to improve the respiration by considering the maintenance of all physiological functions. For that, understanding the flow field within the nose cavity is an essential prerequisite.

The described project investigates the dependency between nose geometry and flow field. In the run-up to a rhinological surgery, an operation planning system, which is integrated into a virtual environment, is to be developed in order to depict differences between the air flow of a healthy nose and the currently treated nose. Virtual surgeries and a connected knowledge database are to result in recommendations for a real surgery. In a first step to build-up this system, the regular flow field is investigated in order to realize what a healthy flow really is. Only thereafter, the know-how can be integrated into a system that advises the surgeon in the preparation of a nose operation.

*gerndt@rz.rwth-aachen.de; phone (+49) 241 / 80 – 20355; fax (+49) 241 / 80 – 22134

In this paper, we mainly describe one of the important components in order to investigate the flow field: the comparison sub-system. We illustrate applied experiments with models of a human nose and how it was used for first numerical simulations. Thereafter, the software application, embedded in a virtual reality framework, is presented. Finally, we describe developed approaches to compute vector field topologies, an outstanding feature to understand and to compare flows.

## 2. EXPERIMENTS AND SIMULATIONS

### 2.1. Experimental Explorations

We need methods to verify the accuracy of numerical simulations. A reliable way is the experimental investigation of flow fields. For this, in cooperation with the clinical center of Aachen, the Aerodynamics Institute of Aachen (AIA) developed models of human nose cavities, whereas the geometry is based on real computer tomography (CT) data. A variety of experiments were applied. For instance, a 3-to-1 model (because of higher resolution of experimental results) consisting of casting resin was constructed. In order to avoid annoying refractions, Tetrahydronaphthalin was used as experimental fluid. Based on this experimental assembly, several optical measuring processes were carried out. The results were stored as images and video sequences (Figure 1, left).

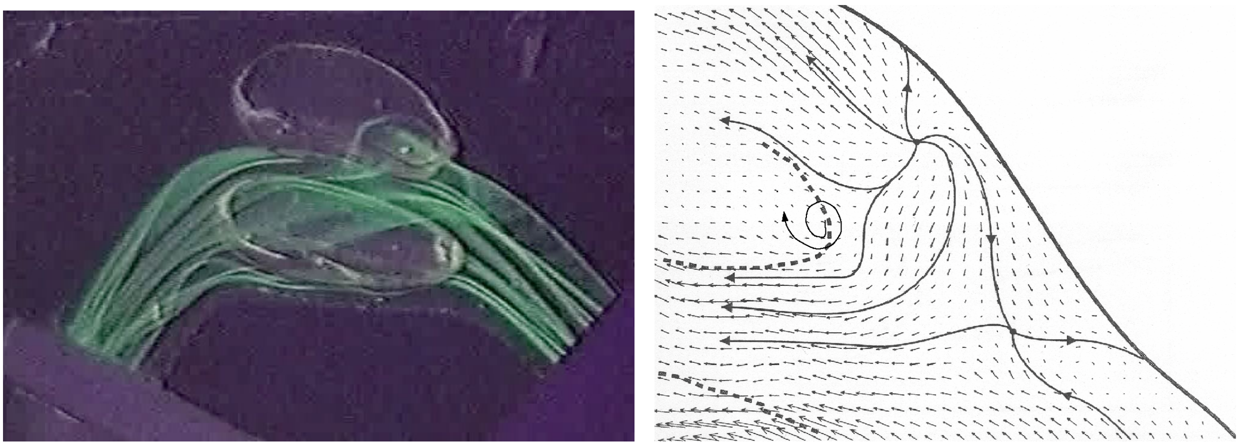

Figure 1. Experiments (left: single video frame, right: Particle Image Velocimetry method).

A more precise experiment is the Particle Image Velocimetry (PIV) method (Figure 1, right). Applying this method, several two-dimensional velocity vector fields on slices parallel to the septum were recorded. The used steady flow volume of 2.5 l/min for inhalation and exhalation corresponds to normal, resting respiration and showed a Reynold number of approximately 650 (based on the entry diameter of the nose cavity). Additionally to this experiment, a number of probes were taken to measure the loss of pressure for different volumes, so that a variety of experimental data was produced for further studies and for the validation of numerical simulations.
The already performed experiments pointed out that modern measurement technology requires more demanding models. Right now, new nose models are constructed being made of silicon. They will be the basis for forthcoming experiments. These model types will also allow water, which is less complicated than the currently used fluid. In the last years, the AIA could gain plenty experiences in using PIV in different areas. This is the reason why future experiments will mainly utilize PIV methods and enhanced approaches like stereoscopic methods [1], holography [2] and Scanning Particle-Image Velocimetry (SPIV) [3]. SPIV is a multi-planar extension of standard PIV that is able to sample the velocity field in all three Cartesian directions over time and with high resolutions.

### 2.2. Numerical Solution

The CT scans were not only used to create artificial noses for experiments but also to generate surfaces of the nose cavity for numerical simulations. *GridPro*, a commercial grid generator, was used to convert these nose surfaces, which consisted of about 400.000 triangles, into a first multi-block grid approximation. Additional modification must be applied in order to adapt the connectivity between cavity and turbinates as well as to improve the multi-block structure. This resulted in 63 blocks with about 150.000 vertices in total. Afterwards, the numerical simulation could be computed by means of Navier-Stokes equations, which were solved by explicit 5-step Runge-Kutta integration.

## 3. SOFTWARE FRAMEWORK

For years, the Virtual Reality Center Aachen (VRCA) has been developing the Virtual Reality (VR) software *ViSTA* [4], which covers all aspects of VR technology. It is scalable in order to integrate all kinds of display systems, ranging from high-end visualization displays like CAVE systems down to standard desktop monitors, and offers a variety of 3D input devices. Special aspects like force-feedback and 3D acoustics are also covered. It is implemented as a toolkit, so that VR applications can be developed rapidly for a specific purpose.

However, *ViSTA* has not integrated scientific visualization and post-processing support. On the other hand, one of the outstanding project areas for the VRCA is scientific visualization, especially for post-processing of Computational Fluid Dynamics (CFD) data sets. Therefore, the VRCA is currently developing an add-on for unsteady flows called *ViSTA FlowLib* [5]. It combines the VR capabilities of *ViSTA* and own research activities in the area of CFD post-processing, which are mainly based on functionalities of Visualization Toolkit (VTK) [6], an object-oriented open-source toolkit developed by a steadily growing community. Since CFD post-processing is generally a time-consuming process, *ViSTA FlowLib* additionally makes use of a parallelization framework called *Viracocha* [7, 8].

### 3.1. The Operation Planning System

With *ViSTA*, *ViSTA FlowLib* and *Viracocha*, a really powerful framework is available. Based on this framework, we are developing a VR-based surgery planning system [9, 10], which integrates different sub-systems. First of all, the planning system integrates a visualization and interaction system for the exploration of three-dimensional nose geometries and their unsteady flows. A multi-modal user interface allows to navigate within the virtual environment and to apply a variety of flow exploration methods. Essential assessment quantities are pressure loss and resting times of particles in the area of the olfactory system.

A next sub-system allows the modification of nose geometries, which is called *Virtual Surgery* even though the goal is to generate a modified mesh for a repeated CFD simulation and not to reproduce the environment of a real nose surgery with all detailed surgery tools. However, the modification should be meaningful with respect to the actual tissue behavior during real human nose operations.

Once modified, the nose surface mesh is exported via an I/O interface back to the flow solver, where the new surface is used to adapt the simulation grid. Thereafter, the restarted CFD simulation computes the caused new flow field. The result is re-imported to the VR system, where again the flow can be explored. If needed, supplementary geometry modifications can be applied, which enforce new CFD simulations. This iterative procedure can be carried out until the respiration flow is satisfying.

However, it is difficult to assess a flow field without comparison possibilities. This introduces the third sub-system: our comparison framework. It allows not only the comparison of different simulation results but also the comparison of experiment vs. experiment as well as experiment vs. simulation. The last one is a popular way to determine the quality of the simulation.

## 4. THE COMPARISON SUB-SYSTEM

In the current project phase, we work with data generated by experiments and simulations that used the artificial nose model described above. Later on, computer tomography data sets of human noses, regular and pathological, as well as CFD simulation data based on real human nose geometries will be imported. However, the used data types are always similar. In case of experimental data, we have to deal with bitmap images, videos and PIV images. The latter are regular two-dimensional grids with velocity vectors at each grid point. When working with numerical simulation data, we are mainly interested in unsteady flow fields, which can be explored by cut-planes (arbitrarily positioned within the 3D data set), iso-surfaces, streamlines and another visualization and extraction algorithms. The extracted data is visualized within the context geometry of the nose currently under investigation. A comparison system has to deal with all these described data types.

### 4.1. CFD Comparisons in Virtual Environments

CFD comparison in virtual environments is not a novel approach. In this section, we briefly give an overview of existing methods to compare experimental data and numerical flow simulations (and among each other) interactively in virtual environments. First of all, we would like to present the concept of comparative visualization, as it was used by [11] and [12] for example.

The main goal of comparative visualization is to emphasize differences between two data sets. It provides a first impression of key differences, which can be highlighted by various visualization techniques. Two-dimensional data are primarily treated by ordinary window-based desktop workstations. In that case, special qualities are often visualized by different color schemes. When dealing with three-dimensional data, the scientist prefers 3D representations on 2D or immersive display devices respectively. At first, useful models for displaying purposes are created by overlapping single data sets or merging several of them into one. The comparison is always done by the user himself.

In 1999, the German Aerospace Research Establishment (DLR) combined stream ribbons extracted from numerical flow simulation data and experimental wind tunnel data [13]. The approach to present different flow phenomena simultaneously gave a better insight into complex flow fields. In another publication [14], comparative visualization in the area of aircraft design was applied to express differences in three-dimensional aircraft models. The main object was the possibility to compare models generated by different tools and methods. The interest was focused on special parts of the models in order to receive knowledge that thereafter could be used for the preparation of the simulation. That should increase the quality of the finally performed simulation.

In 2001, a group of scientists at the NASA Langley Research Center explored the landing gear of a Boing 757 [15]. They carried out experiments in a wind tunnel with a simplified gear model in order to obtain oil-flow data, pressure data, and PIV data. Additionally, seven camera positions were used to receive data for a computer model. This model was displayed within a three-dimensional scene, enriched by the experimental data. Here, they could explore the highly detailed results and detected a variety of features they had not seen in the wind tunnel.

One of the first generally usable VR comparison toolkits was the *Virtual Data Visualizer* (VDV) [16]. It aimed to support visualization of data sets within virtual environments. It offered several interaction methods to scale and animate the displayed data sets. This exploratory data visualization is meant to produce a more in depth sight of complex data content.

Concerning the annotation of data sets, one of the best known systems is the *Virtual Annotation System* [17]. Its goal is to explore and annotate data sets while being immersed in a virtual environment. To manage this work, a great variety of user interfaces are offered. This direct annotation has the advantage of placing markers interactively without the need to switch to a desktop application or using pencil and paper, which both can be very tedious.

### 4.2. Our Approach

Similar to works like immersive studies in the *Virtual Windtunnel* (NASA) and comparative visualization approaches (DLR), we designed a system that allows the use of a variety of interaction and comparison methods within a virtual environment. Traditionally, data comparison is applied on 2D window-based desktop computers or is just performed by watching the video results, while spectators make comments manually. On the other hand, comparative software frameworks running in virtual environments often present only one model at a time for interactive explorations.

***System***

In contrast to these common schemes, we offer a system that allows the free placement of various data sets of arbitrary type within a virtual environment. Appropriate specific information about available data sets is stored in a database. The user has the possibility to select one of the stored data sets that are presented in a list, which will automatically be filled up by the database information. Therefore, direct directory and file browsing is not necessary, which in general would also be a rather unreasonable task in virtual environments. After the choice, the system analyzes the selected data using the stored information and presents it in an adapted *3D context frame* (Figure 2), which provides appropriate functionalities to explore and manipulate the visualized data. These functionalities can considerably differ from each other. For instance, the handling of video data needs buttons to play the animation; and simulation data requires possibilities to select post-processing extractions.

***Interaction / Navigation***

Once loaded, each context frame can be rotated, scaled and moved. The main interaction metaphor is a 3D ball cursor. One can use it to change the context frame location as well as to actuate its control panel. A second metaphor is a wand with an attached 3D beam. For immersive projection systems, more intuitive and accurate interaction metaphors are needed, which is still a demanding and extensive area of research.

One of many approaches we are working on is the usage of a *cutter plane*. This is a hardware device and consists of acrylic glass. Combined with a tracking sensor, it can be used as a direct input device. This is often used, especially during the work with three-dimensional data sets, for instance, to define a cut-plane where scalar values are mapped on or to clip parts of the model in order to obtain a better view to a region of interest. Another hardware device is the phantom haptic device that allows force feedback, for instance, when a button is pressed or a context frame is attached to the wand or cursor ball respectively.

A different approach is the mapping of whole desktop images of 2D window systems onto 3D quadrilaterals that are also located in the virtual environment. This mapping is implemented by texture mapping, which requires a Virtual Network Computing (VNC) server running on the remote window host. Thus, one can use helpful 2D software that is too complex or just impossible (because of licensing, incompatible operating system, etc.) to be converted. Additionally to the mapping of window desktops, we can take along a light-weight tablet PC into the virtual environment to display a complete 2D GUI. Equipped with a tracking sensor, a tablet PC can also be used as a cutter plane, but beyond this possibility a variety of additional functionalities are conceivable.

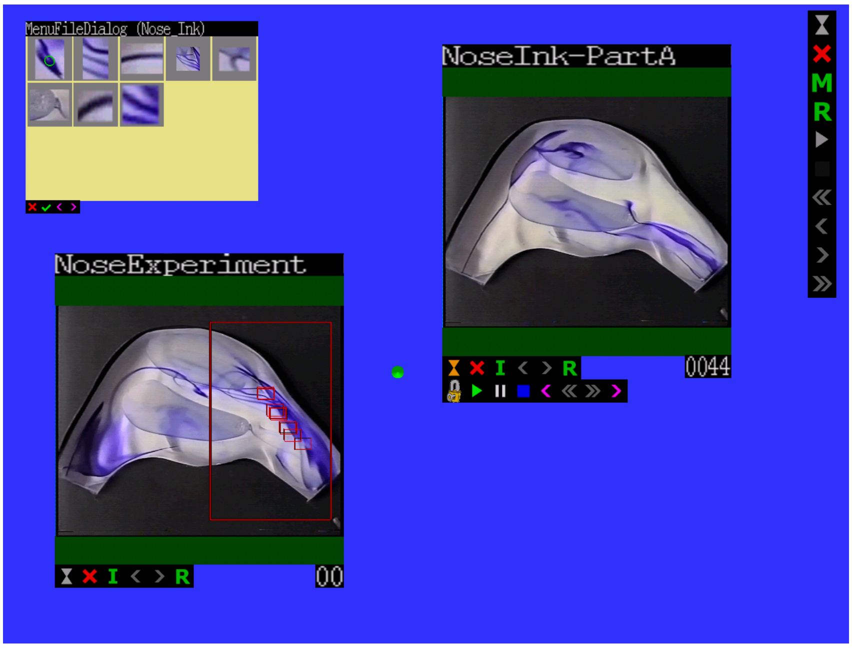


Figure 2. The VR working environment: flow patterns highlighted in one of the selected data sets, context frame for still images (left) and video sequences (right) and 3D ball cursor (mid), global control panel (upper right)

### 4.3. Comparison Schemes

We distinguish two comparison modes: a manual and an automatic mode. In the manual mode, the system enables the scientist to explore, analyze, annotate, and compare data sets simultaneously. In contrast, the second operation mode allows for automatic approaches to find patterns in selected data sets. A straightforward way of comparing two or more images manually is to look at them and write down all differences and recognized special qualities. This is primarily a job for aerodynamics engineers because of the knowledge needed to find specific flow features. However, the comparison sub-system can offer methods to assist the search, e.g. to detect pre-selected patterns in current images.

Possible methods to support the comparative work are manifold; however, the significance of respective procedures heavily depends on the types of currently compared data sets. For instance, images of similar video sequences can easily be compared, but comparing PIV data and images of dye experiments is not meaningful because of their totally different object. Furthermore, recorded results can have different resolutions, dimensions, and colors. Extracted or emphasized flow features could base on different starting conditions, e.g. varying injection points of ink. Supposing the data is comparable at all, comparative approaches have to consider these differences by means of adjustment functionalities.

***Extensibility***

In a first step, we developed the comparison framework with high priority. First comparison methodologies were implemented in order to evaluate the design. One of our main objectives was extensibility. Therefore, a powerful object-oriented framework was developed. In the current implementation, new searching, filtering and comparison algorithms can be added using simple class inheritance. Similar extension possibilities exist for data objects, context frames and menus.

***Overlapping***

Some basic functionality has already been implemented. In addition to comparing data positioned side by side, it is possible to overlap different context frames. This is not restricted to two data sets but can be combined arbitrarily, as long as the merged images allow meaningful observations. This overlapping scheme is primarily based on transparent textures. Therefore, all two-dimensional data sources that present an impression of the complete flow field (like video frames) are suitable for this approach. In contrast, selected cuts need depth information, i.e. they should coincide within the 3D data set; without this requirement, a comparison can be rather inaccurate. A similar problem occurs when visualizing the three-dimensional context geometry of the nose. It is obvious that this geometry is important in order to identify the location of phenomena within the nose, but without depth information, the positioning of 2D cut planes is only vague. However, for most comparisons, this coarse overlapping approach is sufficient.

The depth problem does not occur when using the 3D simulation data set. Here, we always know exactly the position of extracted 3D flow features or selected 2D cuts, so that these extracted data are always visualized in combination with the 3D nose geometry (as wire-frame, or transparent, or as an opaque surface).

***Image Processing***

A first image processing approach to detect flow patterns is based on an average color scheme, which is mainly useful for images or video sequences with similar color distributions. The goal is to find regions in images that match with a pre-selected pattern. These patterns are just image samples taken from other data sets or are created artificially.

The color space we use allows for the human-eye based difference measurement of colors. For that, the data is converted from RGB to CIE L*a*b* color space [18]. The latter, defined by the *Commission Internationale d'Eclairage* (CIE) in 1976, provides a geometrical color distance that is similar to the sensitivity of a human eye. After color space transformation, the search algorithm is applied. It determines an average color value for the used pattern and compares the result with the average color computed for the currently considered region in the image. If the distance between both values is below a threshold, the algorithm has found a hit. The search moves on pixel by pixel by repeatedly applying the pattern color test.

To speed up the search, the pattern is divided into several shells, which are non-overlapping rings of a certain width (Figure 3). First, we start with the inner ring and apply the color test only for pixels covered by this ring. If the test is successful, it is applied for the next adjacent ring. A matching region is detected only if all rings supply hits. Additionally, the rings detect structures of a given pattern, which can also be identified if the pattern is arbitrarily rotated around the center point. As a result, we receive a really fast search to detect features even in a series of images.

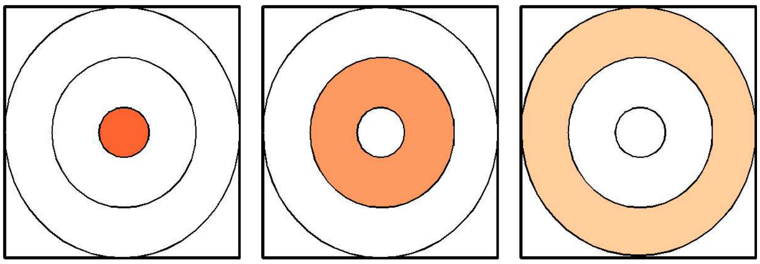

Figure 3. Shells used to identify color thresholds

The comparison system offers a variety of other image processing filters that can be applied directly to data sets. Currently, filters to rotate the image or to flip it along the x-, y-, and z-axis are implemented. Furthermore, the image can be smoothened by the appliance of the Gaussian smooth algorithm. In the near future, other image processing functionalities will be integrated.

***Automatic Pattern Search***

Time dependent video sequences as well as scaled and distorted images make manual comparisons quite difficult. Similar image sequences can appear several times; thus, a reference image or feature cannot be assigned unambiguously. Furthermore, found features in compared images can slightly be moved and are not identified as coincided features. That is why actually matching images are not recognized at all. Without additional support, it would be nearly impossible to determine related images in a large set of similar images in a reasonable time. Therefore, the comparison system also provides automatic search functionalities for feature detection and data comparison. Single images can be inspected by means of image processing methods. In addition to flow features computed by the CFD post-processing, this helps considerably to detect similar structures in images that come from different sources.

For a time dependent search, the user can select single features or a whole image as search parameters. These are used to start a search through a set of images to find a number of candidates of similar images or images that contain requested features. The innovative improvement of our approach is the synchronization feature. It applies a search through one series of images in order to find key-frame candidates that can be used for another series. To detect the related key-frames, not only a single reference frame but a short continuous image sequence can be provided for the matching algorithm. If all matching key-frames are found, both sequences can be played in sync.

### 4.4. The Annotation System

While working with images, the scientist can place them side by side and can mark special characteristics he wants to emphasize. An enhanced annotation system provides a variety of marking functionalities and will be connected to the knowledge database where all comments and findings will be stored. At the moment, we merely store annotation information into plain text files.

We not only record manually placed markers but also support the archiving of previously found flow features. The benefit is that annotations in one data set can give additional information when exploring another data set. An annotation object consists of a marker symbol and an information tag. The marker is a simple geometric object such as a sphere, which can be arbitrarily colored. The information tag can already be defined by the marker type or is an information supplement stored as text or audio data. Since keyboards, in general, are not usable VR input devices, we are also working on speech recognition in order to record short verbal notes. On the other hand, after an immersive VR session, the user has the possibility to utilize a desktop computer for a post-editing of attached annotations.

## 5. VR-BASED POST-PROCESSING

*Vista FlowLib* already offers a variety of standard visualization functionalities to investigate an arbitrary flow. However, our main interest is to provide information about the flow field that allows automatic recognition of essential flow features. Our current research concerns the investigation of vortex theory and critical point extraction. Both approaches are capable of sub-dividing flow fields into distinct sections. These methods are enormous aids to assess the flow behavior within a nasal cavity and should lead to a classification of important nose regions and functions. Stored in a knowledge database, this classification can reveal pathological noses and recommend cavity modifications to remedy diseases.

### 5.1. Two-dimensional Critical Points

Especially for comparison purposes, it is important to consider the 3D flow field only on two-dimensional cuts along the flow direction. Given a cut plane as an implicit function, the resulting mesh consists of arbitrary polygons. Their vertices are the exact intersections with the original data grid and provide interpolated vector and scalar values. In order to simplify further processing steps, each polygon is converted into triangles. Additionally, all velocity vectors are projected onto the plane, which finally results in a flow field presentation comparable to PIV images.

Critical points, also known as singular points or first order stationary points, are positions within the flow field where the velocity magnitude is zero. These are outstanding locations to determine the essential topology of a flow field. Furthermore, streamlines, which describe the trajectory of flow particles, can intersect only at these positions. These special streamlines, called separatrices, divide the vector field into distinct regions. Therefore, critical points and separatrices present the fundamental topology of the considered vector field. [19]

Critical points can be classified related to the way separatrices enter and leave the position. The classification is based on the eigen-analyses of the Jacobian at their locations. The Jacobian $J$ is defined as the partial derivatives at that location; however, because of the discrete kind of the used grid, these derivatives must be approximated by finite differences. The following equation computes the eigenvectors $x$ and the eigenvalues λ where $I$ is the identity matrix:

$$(J - \lambda I)x = 0; \qquad J = \begin{pmatrix} \partial v_x / \partial x & \partial v_x / \partial y \\ \partial v_y / \partial x & \partial v_y / \partial y \end{pmatrix}$$

Equation 1: Computation of eigenvectors and eigenvalues using the Jacobian at the location of a 2-dimensional critical point

We only get a non trivial solution $x \neq 0$ if the determinant of $J - \lambda I$ is exactly zero. Therefore, we just solve the so-called characteristic equation $P_J(\lambda) = J - \lambda I = 0$. For the two-dimensional case, it is straightforward to compute the roots of the characteristic polynom $P_J(\lambda)$. For the three-dimensional case, the computation is more complicated. For higher dimensions, analytical solutions are unreasonable and numerical solutions are preferred.

$$P_J(\lambda) = \lambda^2 + P\lambda + Q = 0$$

Equation 2: The characteristic equation for the two-dimensional case

The computed eigenvalues can be complex numbers. The real term and the imaginary term determine the class of a critical point. If the imaginary part is unequal zero, the eigenvalues are conjugate complex and define a critical point with focal behavior. Otherwise, the critical point is a node with straight streamlines in its neighborhood. The real parts determine the flow direction in the vicinity of a critical point. Positive real terms describe a critical point as source, negative values indicate a sink. If both real terms are zero, the critical point is called a center point. The following table shows the possible classification for the two-dimensional case:

| **Classification** | **Real Terms** | **Imaginary Terms** |
|---|---|---|
| Repelling Focus | R1, R2 > 0 | I1, I2 ≠ 0 |
| Attracting Focus | R1, R2 < 0 | I1, I2 ≠ 0 |
| Center Point | R1 = R2 = 0 | I1, I2 ≠ 0 |
| Repelling Point | R1, R2 > 0 | I1, I2 = 0 |
| Attracting Point | R1, R2 < 0 | I1, I2 = 0 |
| Saddle Point | R1 * R2 < 0 | I1, I2 = 0 |

Table 1: Classification of 2-dimensional first-order critical points

The saddle point is of particular interest. This type of critical point is identified at a location where both computed eigenvalues are not complex and have different signs. We use saddle points in order to compute the separatrices of the flow field. For this, we need the eigenvectors that specify the directions of the four emanating streamlines. These vectors can easily be computed by inserting the already obtained eigenvalues into Equation 1.
The remaining problem is to find the location where the velocity magnitude is zero. Our cut mesh only consists of triangles. Therefore, due to the linearity between arbitrary points within a triangle, it is straightforward to determine the zero position. For this purpose, we use the definition of a triangle by its barycentric coordinates with vertex coordinates $U = (1,0,0)$, $V = (0,1,0)$ and $W = (0,0,1)$. Now, each point within a triangle can be expressed as a point $P = (u,v,w)$, whereas $u+v+w = 1$. Let $x_U$, $x_V$ and $x_W$ be values associated with the vertices, which can be scalars of vectors. Then the following equation computes the corresponding value $x_P$ at the position $P$.

$$x_P = u\, x_U + v\, x_V + w\, x_W$$

Equation 3: Triangle interpolation by means of barycentric coordinates

In our case, we know the value at point $P$, which is zero, and the values at the vertices. Thus, the parameters become the unknowns. Therefore, we have to solve linear system, whereas one of the parameters can be expressed by means of the other two, for instance $w = 1\text{-}u\text{-}v$. These linear equations are easy to solve. If each computed barycentric coordinate is between 0 and 1 and the sum of all is 1, we have found a singular point within the currently considered triangle.

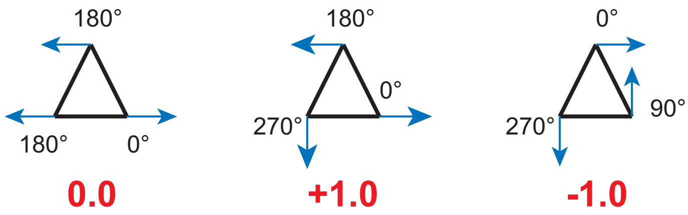


Figure 4: Example triangle patterns and associated Poincaré indices

Solving linear equations for each triangle is rather expensive. Fortunately, one can predict whether a cell contains a critical point or not. For this prediction, we only need the orientation of all three velocity components. Their length and their position are not important; we merely consider the angles between all three vectors. The assessment is based on a concept for vector field topologies introduced by Henry Poincaré. It measures the number of rotations of vectors on a closed curve. Due to linearity, we have to consider only the velocities at the three corners of a triangle. The computed Poincaré index is always 0, 1 or -1. Figure 4 shows some examples of vector orientations and obtained indices. The determined angles are always between 0 and 2π, hence, we can compute the index as follows (compare [20]):

$$PoincareId_{\triangle} = \frac{1}{2\pi}\left(\Delta(\phi_0,\phi_1)+\Delta(\phi_1,\phi_2)+\Delta(\phi_2,\phi_0)\right); \quad \Delta(\phi_i,\phi_j) = \begin{cases} \phi_j-\phi_i+2\pi; & \text{if } \phi_j-\phi_i<-\pi \\ \phi_j-\phi_i; & \text{if } \left|\phi_j-\phi_i\right|\le\pi \\ \phi_j-\phi_i-2\pi; & \text{if } \phi_j-\phi_i>\pi \end{cases}$$

Equation 4: Pointcaré index of a triangle

The important fact is that the Poincaré index is an indicator for singular points. If the index is zero, no critical point is enclosed. In the other case, we found a triangle with an included critical point. Furthermore, we also obtain an indication about the classification of the enclosed point. Exclusively saddle points have index -1 whereas all other yield an index of 1. This is an interesting fact in order to compute the topological graph, since only saddle points are used to determine separatrices [19, 21]. Therefore, if merely the topology graph is of interest, we can reduce computation expenses by determining the eigensystem of saddle points only. A topology result is depicted in Figure 5.

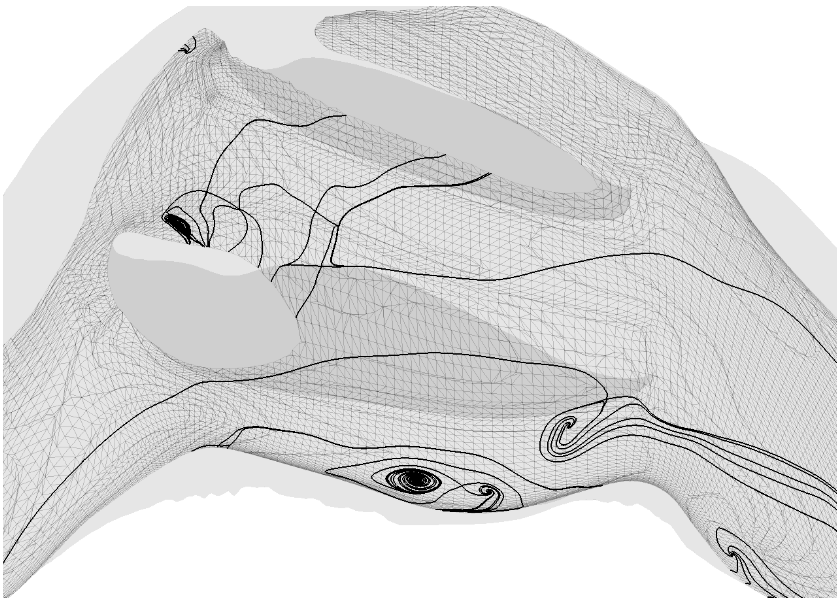

Figure 5: Flow field topology extracted on a cut

However, computing separatices is still expensive. These streamlines are emitted from the saddle point location in positive and negative direction of the corresponding eigenvectors, which merely consist of real components. Therefore, instead of vectors with complex components, they are usable for geometrical utilization. However, computing streamlines starting at seed points with zero start velocities is useless. We need a small offset that, for instance, can depend on the current cell size. Nevertheless, the starting velocity is still low. Accordingly, streamline integration needs a lot of time steps in order to leave the saddle point vicinity. Finally, we have to consider the direction of the start velocity actually taken. This determines whether we need forward or backward integration.

### 5.2. Three-dimensional Critical Points

PIV is a valuable way to obtain measurements of flow experiments on prescribed layers. Other experiments, where special dye like ink is inserted into the flow in order to demonstrate the fluid dispersion, present a flow behavior for the whole three-dimensional domain. The resulting images (single frames or video sequences) are more similar to images received by using simulation results to compute streaklines or streaming surfaces. In that case, the way to use two-dimensional critical points on cuts is not very helpful and sometimes confusing. A more suitable approach for the comparison of simulation vs. experiments is topology extraction in three dimensions.

However, the basic cell type of the 3D nose data set is a hexahedron. Hence, most methods for triangles described for our two-dimensional case cannot be reused. Hexahedrons own linearity only at the edges and on well-defined lines that can be described by means of the tri-linear interpolation. Vice-versa, the interpolation parameters for a given position inside the cell cannot be determined directly. Furthermore, the computation of the position for a given velocity value is not straightforward. For the topology determination we need both: the first to compute separatrices and the latter to search critical points.

For hexahedral grids, Globus [22] recommends to find candidate cells first. For this purpose, we take the first component of a vector and compare it with all other first components of vectors of the same cell. Thereafter, we examine the second and the third components. If all component tests show sign changes (components with positive and negative values exist), a candidate cell is found. This is a necessary condition, but not a sufficient one. Therefore, before any analytical solutions are applied in order to find the position of the stationary point, the cell is subdivided into eight sub-hexahedrons (median cut). The resulting hexahedrons are checked again to be candidates, and thereafter, if required, next bisections are applied. After several iterations, the final position is computed by means of Newton-Raphson interpolation. The reason why it is not applied immediately is the fact that Newton-Raphson needs a good guess for the initial point to converge at all, and it only determines one root. On the other hand, the iterative bisection process converges slowly, but it is successful if a solution exists.

### 5.3. Vortex Extraction

Vector field topology extraction is a convenient way to gain information about the global behavior automatically. An essential element for the classification of critical points is the characteristic equation (see Equation 2), which not only computes eigenvalues but also invariants $P$, $Q$ and $R$ (for the three-dimensional case). These invariants are the basis to compute the discriminant:

$$D = \left( \frac{Q}{3} - \frac{P^2}{9} \right) + \left( \frac{P^3}{27} + \frac{3R - PQ}{6} \right)$$

Equation 5: Discriminant for three-dimensional flow fields

In general, only incompressible flows are considered. Then, $P$ vanishes and the computation for the discriminant can significantly be reduced to $D = 27/4\, R^2 + Q^3$. The interpretation of the discriminant is of particular interest. If we compute iso-surfaces for a discriminant slightly above zero, the resulting surfaces enclose regions of flow that are focally. These regions can also be considered as vortical regions [23].

A more common way to compute vortices is the Lambda$_2$ approach [24]. For this purpose, the Jacobian is divided into its symmetric and asymmetric parts. Thereafter, each part is squared and the result is added up. Now, the eigenvalues of the gained matrix are computed and sorted in increasing order. Afterwards, the second eigenvalue is taken for measurement. If it is negative, the currently considered point belongs to a vortical region. Again, iso-surfaces are extracted to show vortices. The characteristic equation for the Lambda$_2$ approach is depicted as follows:

$$\left((J_s^2 + J_{as}^2) - \lambda\, I)\right) x = 0; \qquad J_s = (J + J^T)/2; \; J_{as} = (J - J^T)/2$$

Equation 6: Determination of eigenvalues for the $Lambda_2$ approach

Critical points, separatrices, vortices computed by means of the discriminate approach and $Lambda_2$ vortices are the main tools we use to provide automatic detection of important flow regions. A snapshot of various features is depicted on Figure 6.

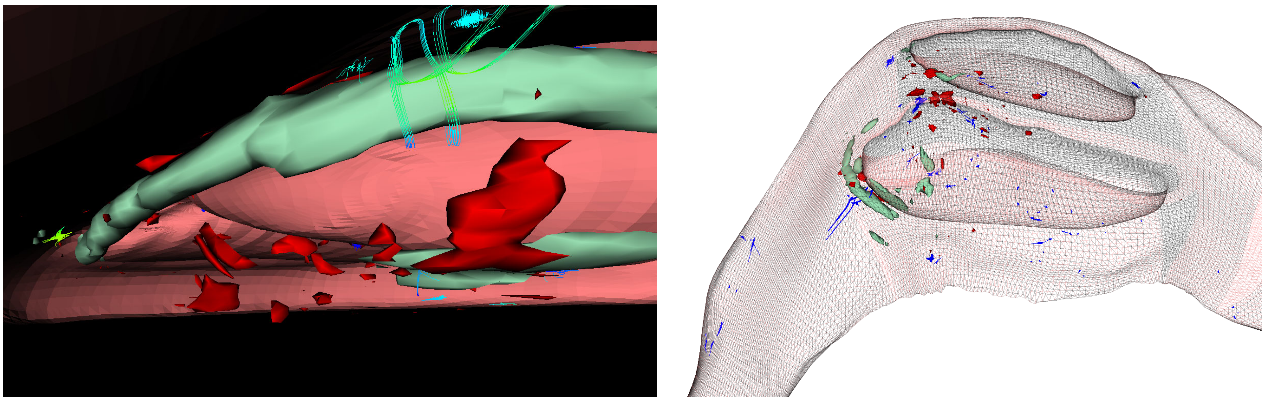

Figure 6: Vortices by discriminants (green) and by $Lambda_2$ (red), enriched by partly computed separatrices; inside (left) and outside (right) view

## 6. CONCLUSION AND FURTURE WORK

The comparison system supports explorative inspection of data from different sources. At the moment, it offers first functionalities in order to detect shared patterns in different still images and video sequences. However, typical features that regularly occur in a flow field of a human nose (healthy or pathological respectively) cannot be searched automatically. It is still necessary that the user pre-selects any samples to search for. In future versions, the system should fall back on a knowledge database filled up with findings collected in previous investigations. The creation of this knowledge database will be one of the most demanding tasks in this project. Only thereafter, the comparison sub-system can detect (semi-automatically) important aspects in a newly loaded data set.

## ACKNOWLEDGE

This work is supported by DFG (German Research Foundation). Additionally, the authors are grateful to the Institute of Aerodynamics, RWTH Aachen University, for the nose data set kindly made available.

## REFERENCES

1. Christoph Brücker, "3-D Scanning Particle Image Velocimetry (3-D SPIV)", In Lecture Notes for VKI Lecture Series Particle-Image Velocimetry, von Karman Institute, Belgium, pp. 1 – 36, 1996
2. R. Konrath, W. Schröder, W. Limberg, "Three-Dimensional Flow Measurements within the Cylinder of a Motored Four-Valve Engine using Holographic Particle-Image Velocimetry", in SAE International Fall Fuels & Lubricants, San Antonio, Texas, 2001
3. Christoph Brücker, "3-D Multiplanar PIV measurements", in M. Riethmuller (editor), "Particle Image Velocimetry and Associated Techniques", VKI Lecture Series, von Karman Institute, Belgium, 2000
4. T. van Reimersdahl, T. Kuhlen, A. Gerndt, J. Henrichs, C. Bischof, "ViSTA: a Multimodal, Platform-Independent VR-Toolkit Based on WTK, VTK, and MPI", Proceedings, 4th International Immersive Projection Technology Workshop, Ames, Iowa, 2000
5. M. Schirski, A. Gerndt, T. van Reimersdahl, T. Kuhlen, P. Adomeit, O. Lang, S. Pischinger, C. Bischof, "ViSTA FlowLib – A Framework for Interactive Visualization and Exploration of Unsteady Flows in Virtual

Environments", Proceedings, 7th International Immersive Projection Technologies Workshop, and 9th Eurographics Workshop on Virtual Environments, Zurich, Switzerland, pp. 77 – 85, 2003
6. W. Schroeder (ed.), "The VTK User's Guide", Kitware Inc., 2001
7. A. Gerndt, T. van Reimersdahl, T. Kuhlen, J. Henrichs, C. Bischof, "A Parallel Approach for VR-based Visualization of CFD Data with PC Clusters", Proceedings, 16th IMACS World Congress, Lausanne, Switzerland, 2000
8. A. Gerndt, M. Schirski, T. Kuhlen, C. Bischof, "Parallel Calculation of Accurate Path Lines using Multi-Block CFD Datasets with Changing Geometry", in: Hamid R. Arabnia, Youngsong Mun (eds.): Proceedings of the International Conference on Parallel and Distributed Processing Techniques and Application, PDPTA'03, Las Vegas, Nevada, USA, pp. 1298 – 1304, 2003
9. T. van Reimersdahl, I. Hörschler, A. Gerndt, T. Kuhlen, M. Meinke, G. Schlöndorff, W. Schröder, C. Bischof, "Airflow Simulation inside a Model of the Human Nasal Cavity in a Virtual Reality-based Rhinological Operation Planning System", Proceedings of Computer-Assisted Radiology and Surgery (CARS 2001), 15th International Congress and Exhibition, Berlin, Germany, pp. 85 – 90, 2001
10. A. Gerndt, T. van Reimersdahl, T. Kuhlen, C. Bischof, I. Hörschler, M. Meinke, W. Schröder, "Large-Scale CFD Data Handling in a VR-Based Otorhinolaryngological CAS-System using a Linux-Cluster", in: Hamid R. Arabnia (Ed.): The Journal of Supercomputing - An International Journal of High-Performance Computer Design, Analysis, and Use, Kluwer Academic Publishers, Issue 2, Volume 25, pp. 143 – 154, 2003
11. Hans-Georg Pagendarm, Frits H. Post, "Comparative Visualization – Approaches and Examples", In Fifth Eurographics Workshop on Visualization in Scientific Computing, May 1994
12. Willem C. de Leeuw, Hans-Georg Pagendarm, Frits H. Post, Birgit Walter, "Visual Simulation of Experimental Oil-Flow Visualization by Spot Noise Images from Numerical Flow Simulation", Technical Report DUT-TWI-95-19, IEEE, Delft, The Netherlands, 1995
13. Hans-Georg Pagendarm, Birgit Walter, "Competent, Compact, Comparative Visualization of a Vortical Flow Field", IEEE Transaction on Visualization and Computer Graphics, 1(2):142-150, June 1995
14. Jens Trapp, Hans-Peter Pagendarm, "Data Level Comparative Visualization in Aircraft Design", in Roni Yagel, George M. Nielsen (editors), Proceedings of the Conference on Visualization, IEEE, Los Alamitos, pp. 393 – 396, 1996
15. Kurt Severance, Paul Brewster, Barry Lazos, Daniel Keefe, "Wind Tunnel Data Fusion and Immersive Visualization: A Case Study", Proceedings of IEEE Visualization 2001, October 2001
16. R. van Teylingen, W. Ribarsky, C. van der Mast, "Virtual Data Visualizer", IEEE Transaction on Visualization and Computer Graphics, 3(1):65-74, January/March 1997
17. Reid Harmon, Walter Patterson, William Ribarsky, Jay Bolter, "The Virtual Annotation System", Proceedings, VRAIS '96, pp. 239 – 245, 1996
18. G. Wyszecki, W. Styles, "Color Science: Concepts and Methods, Quantitative Data and Formulae", Wiley, 1982
19. James L. Helman, Lambertus Hesselink, "Visualizing Vector Field Topology in Fluid Flows", IEEE Computer Graphics and Applications, pp. 36 – 46, 1991
20. Xavier Tricoche, Gerik Scheuermann, Hans Hagen, "Continuous Topology Simplification of Planar Vector Fields", Proceedings, IEEE Visualization, San Diego, CA, 2001
21. Wim de Leeuw, Robert van Liere, "Collapsing Flow Topology Using Area Metrics", Proceedings, IEEE Visualization 99, Los Alamitos, CA, pp. 349 – 354, 1999
22. Al Globus, "Implementation Issues in Vector Field Topology", in Daniel Asimov, Al Globus, Creon Levit (instructors), Tutorial 6, "Vector Field Topology", IEEE Visualization '93, San Jose, California, October 25-29, 1993
23. A. E. Perry, M. S. Chong, "Interpretation of FlowVisualization", in "Flow Visualization – Techniques and Examples", A. J. Smits, T. T. Lim (eds.), Imperial College Press, 2000
24. J. Jeong, F. Hussain, "On the Identification of a Vortex", J. Fluid Mech., vol. 285, Cambridge University Press, 1995